Atom interferometry using Kapitza-Dirac scattering in a magnetic trap

R. E. Sapiro, R. Zhang, and G. Raithel
Department of Physics and FOCUS Center, University of Michigan, Ann Arbor, Michigan 48109, USA
(Received 28 October 2008; published 28 April 2009)

We demonstrate two atom interferometric schemes based on Kapitza-Dirac scattering in a magnetic trap. In the first method, two Kapitza-Dirac scattering pulses are applied with a small time delay between them. High contrast interference is observed both using a thermal cloud and a Bose-Einstein condensate (BEC). In the second method, two Kapitza-Dirac scattering pulses are applied to a BEC with a time separation sufficiently large that the interfering orders complete half an oscillation in the magnetic trap; this enables interferometry between spatially separated paths.

DOI: 10.1103/PhysRevA.79.043630 PACS number(s): 03.75.Dg, 37.25.+k, 37.10.Jk, 67.85.Hj

One of the most promising new technologies suggested by modern atomic physics is atom interferometry. Light interferometers have been used for numerous purposes, including probing materials (for an early example, see Ref. [1]), navigation (for reviews see Refs. [2,3]), and searching for gravitational waves (see Ref. [4] for theory, and Ref. [5] and other Laser Interferometer Gravitational Wave Observatory (LIGO) publications for experimental status). Despite their many uses, however, light interferometers are mostly insensitive to electromagnetic and gravitational fields. Atoms, meanwhile, are sensitive to all of these fields; thus, an atom interferometer can provide a far more sensitive probe of force fields [4], in addition to being able to measure nearly anything a light interferometer can measure. Additionally, if the two arms of an atom interferometer are separately addressable, one can measure atom-surface interactions [6], electric polarizability [7,8], and atom neutrality [9], as well as realize novel nanolithography schemes [10]. In this paper we present the experimental realization of two atom interferometry schemes using Kapitza-Dirac scattering. The first scheme can be used on thermal or Bose-Einstein-condensed (BEC) atoms to produce high-contrast interference patterns with many fringes. The second scheme is used on a BEC to achieve a highly sensitive, large-separation atom interferometer, in which the maximal distance between the BEC components is sufficient that the components can be addressed separately.

Our experimental apparatus for cooling and trapping ^{87}Rb atoms is described in Ref. [11]. The atoms are trapped in an approximately harmonic magnetic potential with a frequency of 45 Hz along the axis of the interferometric arms, and 15 and 45 Hz along the other two axes. We use an optical lattice to create two Kapitza-Dirac scattering pulses for splitting and recombining the atomic wave function. The lattice is composed of a retroreflected laser beam with wavelength $\lambda = 852$ nm and lattice depth of about 80 recoil energies (one recoil energy is equal to $h^2/2\lambda^2 m$, where m is the mass of ^{87}Rb).

When a Kapitza-Dirac scattering pulse is applied to a plane matter wave, the wave function is split into several orders with momenta $2np_r + p_0$, where n is the scattering order, p_0 is the momentum before the Kapitza-Dirac scattering pulse is applied, and p_r is the recoil momentum due to a single photon from the lattice ($p_r = h/\lambda = m \times 5.4$ mm/s). In our experiment, the value of p_0 varies randomly from shot to shot over a range $|p_0| \lesssim 0.4p_r$, due primarily to magnetic field noise. The amplitude of the scattering order n is given by $J_n(V_0 \delta t/\hbar)$, where J_n is the nth-order Bessel function of the first kind, $2V_0$ is the full lattice depth, and δt is the duration of the Kapitza-Dirac scattering pulse [12].

A schematic of the first interferometry scheme is shown in Fig. 1(a). We use two Kapitza-Dirac scattering pulses: one to initially split the atomic wave function into multiple components and the other to recombine some of those components. When we split and recombine the components, we want the resultant interference pattern to arise from the interference of only two components. If more than two components interfere, the pattern becomes more complicated, and thus less straightforward to analyze. We also want the interfering orders to have approximately equal amplitudes, in order to

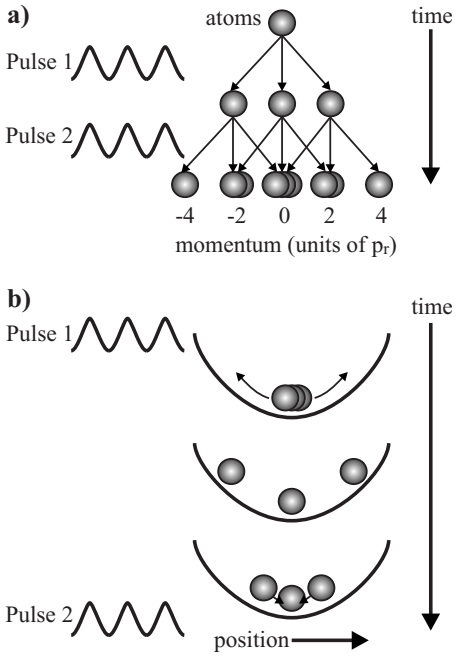

FIG. 1. (a) Schematic of the first interferometry method, represented in momentum space. This method can be used for both a thermal cloud and a BEC. (b) Schematic of the second interferometry method, represented in position space. This method can be used to realize a large-separation atom interferometer.

maximize the visibility of the interference pattern. We choose $\delta t=2$ μs, corresponding to $V_0\delta t/\hbar=1.6$. This causes only a small portion of the wave function to be in orders higher than 1 ($\sim$6% of the wave-function probability is scattered into each of the ± 2 orders), and approximately equal amounts in the -1, 0, and +1 orders. After the application of the first Kapitza-Dirac scattering pulse, a time interval Δt, in the range of hundreds of microseconds, is allowed to pass. During this time, the ± 1 orders move slightly in the trap due to the momentum imparted to them. After Δt, a second Kapitza-Dirac scattering pulse is applied. The wave functions in each order n are split again into several orders n'. After both Kapitza-Dirac scattering pulses, the momentum of a component of the wave function is given by $2(n+n')p_r+p_0$ (neglecting the momentum change due to the magnetic trap). With the second pulse, we again want to coherently split the wave-function components into the orders $n'=0$ and $n'=\pm 1$ with approximately equal amplitudes, while avoiding orders $|n'|\geq 2$. Thus, we also pick $\delta t=2$ μs for the second pulse. Immediately after the second Kapitza-Dirac scattering pulse, the magnetic trap is turned off and the atoms undergo 20 ms of time-of-flight (TOF). During the TOF, the wave function components spread into each other and interfere if they have approximately the same momentum, i.e., if their values of $n+n'$ are equal. If they have significantly different momenta, i.e., their values of $n+n'$ are different, they do not interfere, but rather gain macroscopic separation during TOF.

The description in the previous paragraph applies to a single atom interfering with itself. However, the experiment can be performed on a thermal cloud cooled to a sufficiently low temperature. At very low temperatures, the atoms in the thermal cloud will have similar enough momenta that even though the resulting measurement is an incoherent sum over all of the atoms, the interference pattern can still be seen [13]. We perform this experiment on a thermal cloud consisting of $(2-3.5)\times 10^5$ atoms evaporatively cooled to just above the BEC transition. The results for various delay times Δt are shown in Fig. 2(a). As can be seen, interference fringes are clearly visible up to $\Delta t=400$ μs. At image positions corresponding to momenta $\pm 2p_r$ in Fig. 2(a), two wave-function components interfere with each other, namely, the components $(n,n')=(0,\pm 1)$ and $(\pm 1,0)$. As a result, at these image positions the interference patterns exhibit regular, sinusoidal interference fringes. The fringe contrast varies with Δt; at $\Delta t=50$ μs a fringe contrast of over 90% is observed, while at $\Delta t=400$ μs the fringe contrast is only 33%. At the center of the images in Fig. 2(a), three wave function components interfere with each other, namely, $(n,n')=(0,0)$, $(1,-1)$, and $(-1,1)$, resulting in more complicated interference patterns. The interference patterns near zero momentum are most visibly complex when the fringe period is largest, at small Δt.

To obtain the fringe period, λ_f, from our experimental data, we determine the average distance between adjacent peaks for a given Δt, using multiple images, and ignoring the center region where the fringe pattern is more complex. The resulting plot, λ_f vs $1/\Delta t$, is shown in Fig. 2(b). The error bars shown in the figure are based on estimated reading uncertainties, due to camera resolution, and the number of

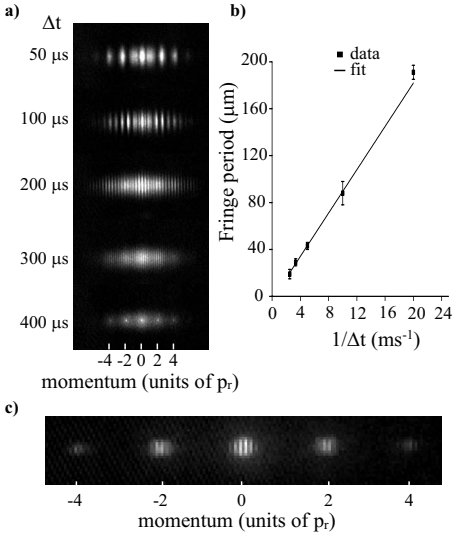

FIG. 2. (a) Thermal-cloud interference with different time intervals, Δt, between Kapitza-Dirac scattering pulses. (b) Fringe period of interference for a thermal cloud vs $1/\Delta t$. (c) BEC interference, for $\Delta t=420$ μs between pulses.

samples. Applying a linear fit, we find a slope of 9.2 μm ms, with a fit uncertainty of ± 1.1 μm ms.

The fringe period can also be calculated analytically and using simulations. To find λ_f analytically, we assume the wave function is initially in the ground state of the harmonic potential (frequency $\omega=2\pi\times 45$ Hz in our experiment). The first Kapitza-Dirac scattering pulse splits the wave function into several components with momenta differing by multiples of $2p_r$. Since the harmonic trap is left on between the Kapitza-Dirac scattering pulses, these components propagate without dispersion and maintain a position uncertainty of $\sigma=\sqrt{\hbar/2m\omega}$. The expectation values of the positions and momenta of the components follow the classical equations of motion of the harmonic oscillator. The second Kapitza-Dirac scattering pulse, applied at time Δt, then splits the evolved wave-function components a second time. After the second Kapitza-Dirac scattering pulse the harmonic-oscillator potential is turned off, and the wave function components propagate according to the well-known equation for a free Gaussian wave packet,

$$\psi_l(x,t)\propto\frac{\exp(ik_lx-iE_lt/\hbar)\exp\left(\frac{-(x-x_l-\hbar k_lt/m)^2}{4\sigma^2[1+i\hbar t/(2\sigma^2m)]}\right)}{\sqrt{2\pi[1+i\hbar t/(2\sigma^2m)]}}. \quad (1)$$

Here, x_l and k_l are the expectation values of the position and momentum of component l immediately after the second Kapitza-Dirac scattering pulse, E_l is the energy of component l, and t is the time elapsed after turning off the harmonic potential. The interference pattern after time of flight is obtained by setting $t=t_{TOF}$ and summing over all wave-packet components. Specifically, the periodicity λ_f of the interference pattern in the overlap region of two components, $l1$ and $l2$, follows:

$$2\pi/\lambda_f = \left| \frac{\partial \phi_{l1}}{\partial x} - \frac{\partial \phi_{l2}}{\partial x} \right|, \tag{2}$$

where ϕ_{l1} and ϕ_{l2} are the phases of wave-packet components $l1$ and $l2$. After extracting $\phi_{l1}(x,t)$ and $\phi_{l2}(x,t)$ from Eq. (1) and taking the spatial derivatives, Eq. (2) leads to

$$\lambda_f = \frac{2\pi}{m}\left(\frac{4m^2\sigma^4 + \hbar^2 t_{TOF}^2}{-4mk_{rel}\sigma^4 + \hbar t_{TOF} x_{rel}} \right), \tag{3}$$

with $k_{rel}=k_{l2}-k_{l1}$ and $x_{rel}=x_{l2}-x_{l1}$. Maximum interference contrast occurs at the classical intersection time of the wave packets, $t_{class}=-mx_{rel}/(\hbar k_{rel})$; as expected, the fringe period λ_f at that time equals $\lambda_{class}=2\pi/k_{rel}$. Since the wave packets spread considerably during time of flight, for values of t_{TOF} different from t_{class} there can still be high-contrast interference, with fringe periods λ_f different from λ_{class}. To find λ_f for our experiment, we may consider, for instance, the interference of the scattering orders $(n,n')=(0,1)$ with $(n,n')=(1,0)$. For these, $k_{rel}=2k_L[\cos(\omega\Delta t)-1]$ and $x_{rel}=(2p_r/m\omega)\sin(\omega\Delta t)$. It is easy to verify that under the conditions of Fig. 2 the terms in Eq. (3) that involve σ are much smaller than the terms that involve the time of flight, t_{TOF}. Noting further that under the conditions of Fig. 2, $\omega\Delta t \ll 1$, and thus $x_{rel} \approx 2p_r\Delta t/m$, we arrive at

$$\lambda_f \approx \frac{ht_{TOF}}{2p_r\Delta t}. \tag{4}$$

This is the same equation as given in Ref. [13] for the case of free evolution between pulses and in the absence of mean-field interaction. Thus, in this first interferometry scheme, where $\omega\Delta t \ll 1$, the presence of the harmonic trap between the Kapitza-Dirac scattering pulses has no significant effect on the fringe period. According to Eq. (4), in our system we expect $\lambda_f = \frac{1}{\Delta t} \times 8.5$ μm ms. This is in reasonable agreement with our experimental observations.

The modeling described so far has been restricted to the case where the initial wave function is in the ground state, whereas the experiments discussed so far have been performed on thermal clouds. A thermal cloud of atoms at temperature T in a harmonic oscillator (frequency ω) can be modeled as an ensemble of minimum-uncertainty Gaussian wave packets with average initial positions x_t and momenta k_t following thermal distributions, $\omega^2 m\langle x_t^2\rangle = \hbar^2\langle k_t^2\rangle/m = k_B T$. Forming weighted averages of the interference patterns produced by such wave function ensembles we find that high-contrast interference patterns may be observed for temperatures up to hundreds of nK. We have qualitatively confirmed this finding in the experiment by varying the temperature T of the cold-atom cloud. We control the temperature by stopping the rf-induced evaporative cooling at different frequencies above the critical frequency at which a BEC begins to form. We determine the resultant temperature of the thermal cloud, after evaporative cooling and adiabatic relaxation of the magnetic trap, using TOF analysis along the vertical direction of the shadow images. We experimentally observe interference for temperatures up to $T \sim 650$ nK. Due to uncertainties in the size of the initial atom cloud before TOF, the uncertainties of the temperature measurements are

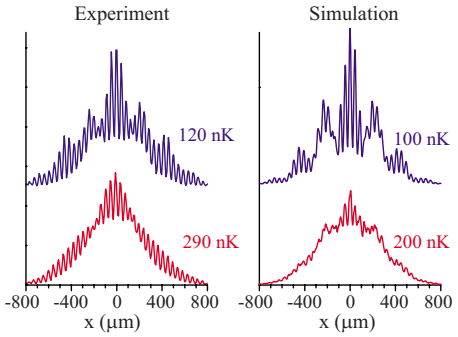

FIG. 3. (Color online) Experimental and simulated interference patters for $\omega=45$ Hz, $\Delta t=200$ μs, $t_{TOF}=20$ ms, and the indicated temperature values. Experimental temperatures are estimated using TOF, and have uncertainties of ± 50 nK.

~ 50 nK (which corresponds to a fairly high relative uncertainty for the lowest temperature thermal clouds). In Fig. 3 we compare experimental interference patterns obtained with thermal samples to simulated patterns (simulated for the temperatures indicated in the figure), and find some qualitative agreement. However, the experimental results at high temperatures show greater fringe contrasts than the simulations; we still see contrasts of 13% at ~ 650 nK in the experiment, but the simulations indicate that the interference pattern should be completely washed out at that temperature. This parallels the observation of Miller *et al.* in Ref. [13]. Their proposed explanation of velocity-selective Bragg diffraction does not fit our experiment, though, since Kapitza-Dirac scattering is not velocity selective.

We have also implemented the described interferometry scheme using BECs of $(5-8)\times 10^4$ atoms. Since the spatial extent of the BEC components after time of flight is much smaller than that of cold thermal clouds, it is more challenging to observe interference in BECs than in cold thermal clouds. Fringes in BECs can only be observed if the fringe period, λ_f, is less than the size of the BEC components after TOF, but still larger than the spatial resolution of the imaging system (which is ~ 7 μm in our experiment). In our system, these contrasting requirements mean that BEC interference fringes can only be observed over the range 300 $\mu s \lesssim \Delta t \lesssim 800$ μs. In Fig. 2(a) we see that in the case $\Delta t=400$ μs, where there is a mix of thermal cloud and a very small BEC, a single interference fringe is only slightly smaller than a BEC component. In Fig. 2(c), we show BEC inteference for $\Delta t=420$ μs; several interference fringes are visible in each BEC component. For $\Delta t \lesssim 300$ μs, the interference fringes are too wide to be visible, but any asymmetry between the paths of the +1 and −1 components will still cause a phase shift in the interference. These phase shifts manifest as one component having a greater amplitude than its symmetric component in the TOF image. An example leading to asymmetry between the paths of the +1 and −1 components is the initial momentum of the wave function, p_0. In our system, variations in the magnetic trapping fields cause a shot to shot fluctuation of p_0 over a range $|p_0| \lesssim 0.4p_r$. The resulting asymmetry in the interference pattern can be quantified by comparing the number of atoms P_- and P_+ with momenta $-2p_r$ and $+2p_r$, respectively, in the

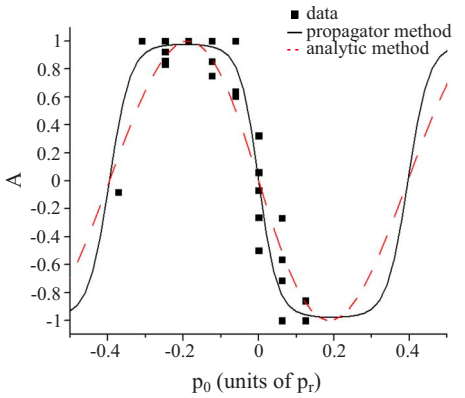

FIG. 4. (Color online) Asymmetry between the number of BEC atoms with a final momentum $+2p_r$, P_+, and the number of BEC atoms with a final momentum $-2p_r$, P_-, defined by $A=\frac{P_+-P_-}{P_++P_-}$, as a function of the initial momentum p_0, for $\Delta t=100$ μs. Squares are experimental data; solid line is a simulation based on propagators; dashed line is an analytic calculation, following Eq. (5).

TOF images. In the presence of a cold thermal cloud, p_0 can be measured by using the interference of the thermal cloud as a reference. A thermal cloud has a sufficiently wide range of initial momenta that its interference pattern is independent of small variations in the average momentum. Thus, the center of the thermal-cloud interference pattern can be taken as $p=0$. The initial momentum of the BEC can then be found by comparing the position of the BEC component with $n+n'=0$ to the $p=0$ position as indicated by the thermal cloud. A straightforward calculation shows that, in the limit of small Δt and weak Kapitza-Dirac scattering ($V_0\delta t/\hbar \ll 2.4$), the asymmetry of P_- and P_+, defined as $A=(P_+-P_-)/(P_++P_-)$, should vary as

$$A=\frac{-\sin(2\hbar\Delta t k_L^2/m)\sin(2\hbar\Delta t k_L k_0/m)}{1+\cos(2\hbar\Delta t k_L^2/m)\cos(2\hbar\Delta t k_L k_0/m)}, \tag{5}$$

where $k_L=2\pi/\lambda$ and $k_0=p_0/\hbar$. Using simulations, we have found that for $\delta t=2$ μs (the value used in the experiments) Eq. (5) approximately holds for lattice depths, $2V_0$, of up to about 70 recoil energies; for deeper lattices the dependence of A on Δt and k_0 becomes more complicated due to higher-order scattering. Therefore, to model our experiment, where the lattice depth is about 80 recoil energies, we use a numerical simulation. In Fig. 4, we plot A as a function of p_0 for images containing both a BEC and a thermal cloud with $\Delta t=100$ μs (squares), the simulation using propagators (solid line), and the analytic calculation [Eq. (5); dashed line]. Since the lattice depth is large, the analytic method does not accurately describe our experiment. The experimental data do agree well with the theoretical result based on propagators, showing that the experimental shot-to-shot variations in p_0 result in well-characterized changes of the interferometric quantity A.

The second interferometry scheme demonstrated in this paper differs from the first in that Δt is more than an order of magnitude larger: ~8 ms. This allows the nonzero momentum components produced by the first Kapitza-Dirac scattering pulse to complete a half-oscillation in the magnetic trap

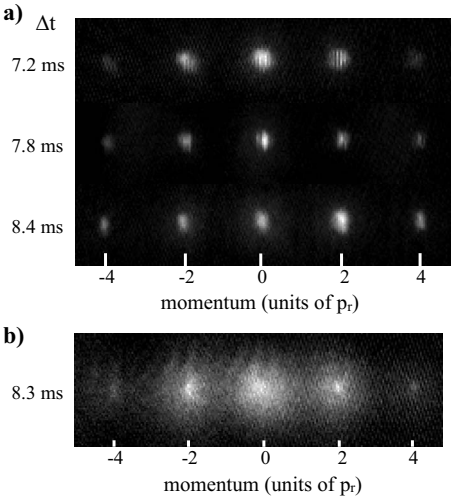

FIG. 5. Large-separation atom interferometer. After undergoing a half-period oscillation in the magnetic trap: (a) BEC interference can clearly be seen for various Δt; (b) a thermal cloud shows weak interference ($\Delta t=8.3$ ms).

and return approximately to their initial positions near the center of the trap by the time the second Kapitza-Dirac scattering pulse is applied. This procedure, a schematic of which is shown in Fig. 1(b), is a realization of a Mach-Zehnder interferometer. In the present work, clear demonstrations of this interferometer have only been possible using BECs. Under our experimental conditions, the +1 and −1 BEC components (starting with momenta of about $+2p_r$ and $-2p_r$, respectively) are, at the farthest point, 60 μm apart, which is much larger than the BEC size. This is far enough apart that it would be possible to manipulate the atoms traveling in one arm of the interferometer without affecting the atoms in the other; for example, a distance of 60 μm can be resolved using laser beams. The sensitivity of an atom interferometer to accelerations and fields is proportional to Δt. While a few other groups have achieved larger Δt (see, for example, Refs. [14,15]), 8 ms is still one of the larger time separations [16].

The images shown in Fig. 5, taken as described above, demonstrate that our large-separation interferometer produces interference fringes after a half-round-trip of the atoms in the magnetic potential (for the case depicted in Fig. 5, the frequency of the trap along the axis of the lattice is 60 Hz). The contrast of these fringes varies considerably from shot to shot, ranging from 20% to 75%. In the large-separation interferometer, the fringe period is no longer described by Eq. (4) because $\omega\Delta t$ is not $\ll 1$. At $\Delta t=8.4$ ms, very close to a half-oscillation in the magnetic trap, λ_f is larger than a BEC component, and interference is observed indirectly as a difference in atom number between the components emerging with $\pm 2p_r$, as described above for the other interferometry scheme. As seen in the figure, the +1 component has a larger population than the −1 component. At 7.2 ms and 7.8 ms, λ_f is small enough that multiple fringes can be seen in each BEC component. The presence of multiple fringes theoretically allows for more sensitive measurement, in that small changes in the phase of the fringes can be observed, rather than the less precise measurement of the number of atoms in each component. In order to exploit this potentially higher

sensitivity, however, it would be necessary for the imaging system to be able to resolve small phase changes, which is not the case in our present setup.

The mean-field energy of the BEC in our system is $\sim h \times 100$ Hz, so in theory it should be possible to begin to see small effects from the mean field after a half oscillation. However, although the number of atoms in our BEC varies by a factor of about 2, we see no correlation between atom number and fringe phase when we compare images with the same p_0. When we simulate the interferometer and vary the mean field, we find that for the range of BEC sizes in our experiment, we would expect the variation in the fringe position due to the mean field to be smaller than the resolution of our camera, e.g., ~ 5 μm for the case of $\Delta t = 7.8$ ms. The simulations show a systematic shift of ~ 10 μm, however, between a BEC of the size of the ones used in our experiment and one with an order of magnitude fewer atoms.

While our spatial and temporal separations are not as large as those in the experiment of O. Garcia *et al.* [14] (who hold the record for a BEC interferometer with the arms completely spatially separate), our system provides some advantages over theirs. One advantage is that we can make λ_f small enough to see individual fringes by making Δt not exactly equal to half an oscillation period in the magnetic trap. As mentioned above, this allows for potentially more precise measurements. Another advantage is that we use the curvature of our magnetic trap as the "mirrors" at the end of each arm of the Mach-Zehnder interferometer. This is both easier to implement and more reproducible than using a Bragg-scattering pulse. A Bragg-scattering pulse can lose its efficiency if the BEC starts with a small unknown momentum, as is the case for both our experiment and the one described in Ref. [14], while a small momentum has no effect on the efficiency of a Kapitza-Dirac pulse. Additionally, Kapitza-Dirac scattering provides advantages over Bragg scattering for interferometers where the arms are separate for only a short period of time. Bragg-scattering pulses are much longer than Kapitza-Dirac scattering pulses, and in many cases may take up a sizable portion of the separation time (for example, [13]).

Based on the periodicity of the propagator of the one-dimensional harmonic oscillator, for given Δt_0 and integer n one would expect to find the same shadow images for all values $\Delta t = \Delta t_0 + n\pi/\omega$. Thus, based on observations of thermal-could interference at some short-time delay, $\Delta t_0 \lesssim 500$ μs, as in Fig. 2, one might expect to find similar interference patterns of thermal clouds at much longer delay times, $\Delta t = \Delta t_0 + n\pi/\omega$. We observe that cold, thermal clouds do indeed produce some interference after a half-round-trip, as demonstrated in Fig. 5(b). Nonetheless, in all cases studied the thermal-cloud interference observed after a half-round-trip has been found to be much less pronounced than after short-time delays, $\Delta t \lesssim 500$ μs. The observed fringe contrast is 35% along the top edge of the shadow image, while it drops to zero near the center line and below. There are multiple causes that can explain the discrepancy between this observation and the high-contrast fringes observed for a BEC after the same time delay. The motion of the atoms in the trap may not be exactly one-dimensional. If the lattice laser is not perfectly aligned with one of the principal axes of the trap, the components gain a small momentum along a transverse axis of the trap. In this case, the interference planes in three-dimensional space may tilt after a large Δt due to differences in trap frequency along the different axes of the trap. This would cause the interference to average out in the shadow images, which are two-dimensional projections of the atom density. This is also the probable cause of the noticeable tilting of the fringes in Fig. 5(b). Additionally, any anharmonicity of the trap potential would break the periodicity of the propagator, leading to a reduction in the coherence time of cold, thermal samples.

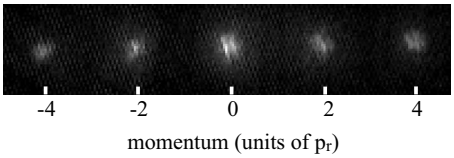

FIG. 6. Interference after a full-period oscillation. $\Delta t = 16.5$ ms.

Finally, as an extension of the previous scheme, we demonstrate that interference can be seen when the ± 1 components are allowed to undergo a full oscillation. This is shown for a BEC in Fig. 6, where $\Delta t = 16.5$ ms. In this case, the fringes appear tilted; this is presumably because the lattice laser is not perfectly aligned with the axes of the trap, as explained above. The full-oscillation version of the large-separation interferometer has both advantages and disadvantages over the half-oscillation version presented above. Having both components go through all the same space over the course of their separation negates any phase difference a component might pick up due to asymmetries in the trap. Time-independent, spatially dependent fields and linear accelerations would affect both components equally, since they each sweep out the same spatial range. Each component is separately addressable only if the duration of the perturbation under investigation is timed such that it affects one component when it reaches one end of the trap but is no longer present by the time the other component reaches that location. Furthermore, when the ± 1 components collide at the center of the trap after half an oscillation, atom loss and four-wave mixing can occur due to s-wave scattering.

In conclusion, we have presented two simple atom interferometry schemes using Kaptiza-Dirac scattering. In one scheme, we can produce large, high-contrast interference fringes in both a BEC and a thermal cloud. In the other scheme we can see visible interference fringes after the BEC components follow spatially separated paths. This separation is sufficient for the BEC components to be individually addressable.

We acknowledge the support of AFOSR (Grant No. FA9550-07-1-0412) and FOCUS (NSF Grant No. PHY-0114336).

[1] A. Bramley, J. Franklin Inst. **203**, 251 (1927).
[2] E. J. Post, Rev. Mod. Phys. **39**, 475 (1967).
[3] B. Culshaw, Meas. Sci. Technol. **17**, R1 (2006).
[4] L. Stodolsky, Gen. Relativ. Gravit. **11**, 391 (1979).
[5] B. Abbott, R. Abbott, R. Adhikari *et al.*, Phys. Rev. D **76**, 082003 (2007).
[6] J. D. Perreault and A. D. Cronin, Phys. Rev. Lett. **95**, 133201 (2005).
[7] C. R. Ekstrom, J. Schmiedmayer, M. S. Chapman, T. D. Hammond, and D. E. Pritchard, Phys. Rev. A **51**, 3883 (1995).
[8] A. Miffre, M. Jacquey, M. Büchner, G. Trénec, and J. Vigué, Phys. Rev. A **73** 011603(R) (2006).
[9] A. Arvanitaki, S. Dimopoulos, A. A. Geraci, J. Hogan, and M. Kasevich, Phys. Rev. Lett. **100**, 120407 (2008).
[10] A. Gangat, P. Pradhan, G. Pati, and M. S. Shahriar, Phys. Rev. A **71**, 043606 (2005).
[11] R. Zhang, R. E. Sapiro, N. V. Morrow, R. R. Mhaskar, and G. Raithel, Phys. Rev. A **77**, 063615 (2008).
[12] P. L. Gould, G. A. Ruff, and D. E. Pritchard, Phys. Rev. Lett. **56**, 827 (1986).
[13] D. E. Miller, J. R. Anglin, J. R. Abo-Shaeer, K. Xu, J. K. Chin, and W. Ketterle, Phys. Rev. A **71**, 043615 (2005).
[14] O. Garcia, B. Deissler, K. J. Hughes, J. M. Reeves, and C. A. Sackett, Phys. Rev. A **74**, 031601(R) (2006).
[15] G.-B. Jo, Y. Shin, S. Will, T. A. Pasquini, M. Saba, W. Ketterle, D. E. Pritchard, M. Vengalattore, and M. Prentiss, Phys. Rev. Lett. **98**, 030407 (2007).
[16] Ying-Ju Wang, Dana Z. Anderson, Victor M. Bright, Eric A. Cornell, Quentin Diot, Tetsuo Kishimoto, Mara Prentiss, R. A. Saravanan, Stephen R. Segal, and Saijun Wu, Phys. Rev. Lett. **94**, 090405 (2005).